BIOMIMETICS

A controllable dual-catapult system inspired by the biomechanics of the dragonfly larvae's predatory strike

Sebastian Büsse*, Alexander Koehnsen, Hamed Rajabi, Stanislav N. Gorb

The biomechanics underlying the predatory strike of dragonfly larvae is not yet understood. Dragonfly larvae are aquatic ambush predators, capturing their prey with a strongly modified extensible mouthpart. The current theory of hydraulic pressure being the driving force of the predatory strike can be refuted by our manipulation experiments and reinterpretation of former studies. Here, we report evidence for an independently loaded synchronized dual-catapult system. To power the ballistic movement of a single specialized mouthpart, two independently loaded springs simultaneously release and actuate two separate joints in a kinematic chain. Energy for the movement is stored by straining an elastic structure at each joint and, possibly, the surrounding cuticle, which is preloaded by muscle contraction. As a proof of concept, we developed a bioinspired robotic model resembling the morphology and functional principle of the extensible mouthpart. Understanding the biomechanics of the independently loaded synchronized dual-catapult system found in dragonfly larvae can be used to control the extension direction and, thereby, thrust vector of a power-modulated robotic system.

INTRODUCTION

Throughout all animal groups, predator-prey relationships can cause an evolutionary arms race, which can lead to the development of elaborate biomechanical mechanisms. For example, an adaptation in a predator can change the selection pressure on its prey, possibly leading to a counteradaptation and vice versa—if these processes alternate, we talk about an arms race (*1*). Some of these mechanisms rely on very fast movements (ballistic movements), for example, in prey capturing or jumping [the latter typically used as an escape mechanism (*2*–*6*)]. Muscles can either generate a high force or achieve high contraction speeds, yet the power output of muscles has a limit. Especially in small animals such as insects, extreme accelerations are necessary to quickly achieve high speeds. This requires both fast muscle action and high force output, a requirement exceeding the maximum power output of muscles. The mechanical power output is therefore modulated to a degree far surpassing the maximal power of a muscle (*7*–*10*) by releasing energy that has been previously stored in elastic structures (*7*, *11*). In many cases, these ballistic movements are enabled by a catapult mechanism [also referred to as latch-mediated spring actuation (LaMSA) in (*12*)], where a spring is locked in position and slowly preloaded (for example, via muscle contraction). The stored energy is released almost instantaneously via a trigger mechanism (*11*); a catapult system such as a slingshot is a simple example.

The escape jump of froghoppers [Insecta: Cicadomorpha (*4*, *6*)] is one example of these complex movements. Here, a catapult-like elastic mechanism performs one of the fastest jumps known, by using chitinized cuticle as a spring (*3*). The elastic protein resilin, using the energy of the jump, rapidly returns the leg to its original shape after a jump and allows for repeated jumping (*6*). Resilin represents a cuticular component (protein) of high resilience, low fatigue, and damping mechanisms in arthropods (*13*) due to its viscoelastic properties (*14*). In the specific case of a catapult system, the near-perfect resilience (92 to 97%) and a fatigue limit of over 300 million cycles (*15*), in combination with the ability to stretch to over three times its original length and recoil to its initial state without plastic deformation (*16*, *17*), become important.

Our example is the predatory strike that Odonata larvae (those of dragonflies and damselflies) use to capture prey, such as invertebrates, as well as small vertebrates such as tadpoles and fish up to their body size (*18*), in freshwater habitats. They evolved a strongly modified, extensible mouthpart called prehensile labial mask (Fig. 1A) (*19*, *20*), which they project toward prey during an ambush [see movie S1 (*20*)]. Previous investigations concluded that the protraction of the extensible mouthpart (prehensile labial mask) is primarily driven by hydraulic pressure (*21*–*25*). Through the compression of the strong abdominal dorsoventral muscles in a rectal chamber, also used for respiration, pressure is generated and a water jet is ejected, propelling the larvae forward (*26*, *27*). The latter so-called jet propulsion represents a special escape behavior similar to that of squids (*28*). For the predatory strike, this pressure is supposedly redirected and used for the protraction of the extensible mouthpart (*21*–*25*). A combination of hydraulic pressure and co-contraction of the power muscles as the driving force for the predatory strike was previously suggested by Tanaka and Hisada (*24*); however, they conducted electrophysiological experiments with no muscle being active during the protraction of the mask (see details below). In addition, muscle dissection experiments (*24*) and the presence of specialized morphological structures resembling a locking mechanism (*29*) suggest the necessity of a reinterpretation of the entire system [see also (*30*)].

We present evidence for an independently loaded synchronized dual-catapult system (ILSDC) as the driving force of the predatory strike in dragonfly larvae. The energy provided by the rather slow contraction of muscles is stored through the deformation of two cuticular structures. These two catapults are connected by a joint and operate together as a two-link kinematic chain (Fig. 1B) to allow for the previously mentioned power modulation. We show that the power output required to achieve the observed angular acceleration of the extensible mouthpart (prehensile labial mask) of dragonfly larvae exceeds the power output achievable by the associated musculature

Department of Functional Morphology and Biomechanics, Institute of Zoology, Kiel University, Am Botanischen Garten 9, 24118 Kiel, Germany.
*Corresponding author. Email: sbuesse@zoologie.uni-kiel.de

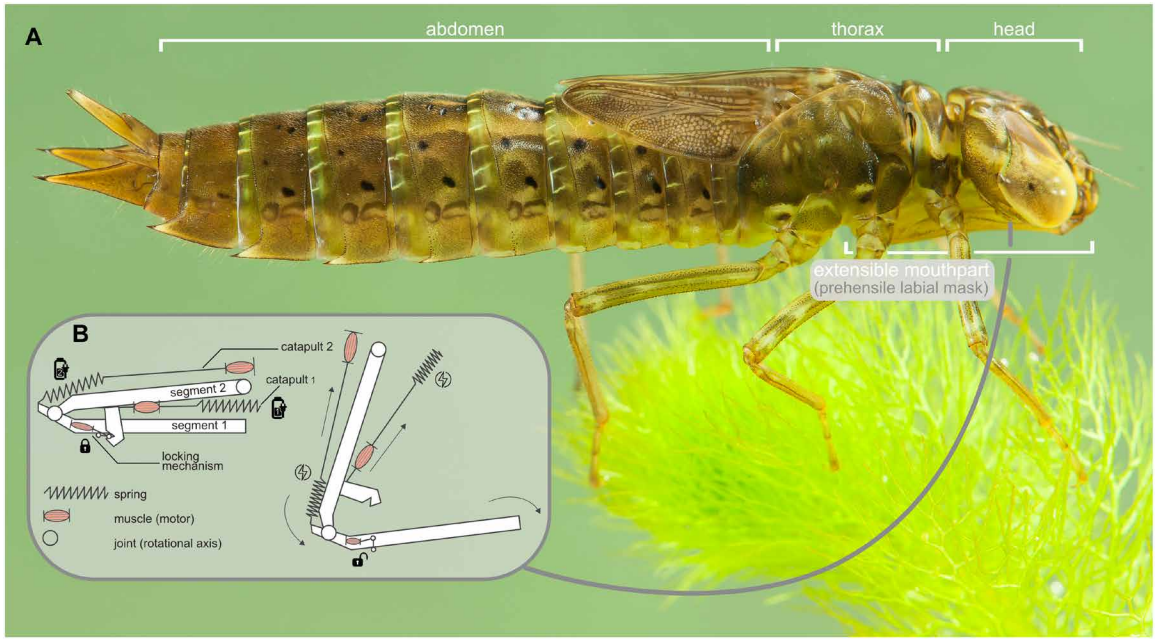

Fig. 1. Dragonfly larva. (**A**) Lateral view of *Anax imperator* (Odonata: Anisoptera). Photo credit: Christophe Brochard/Brochard Photography. (**B**) Abstract principle of the ILSDC concept.

(*8*–*10*). This finding implies that a purely muscle-driven movement is unlikely, given our current understanding of muscle physiology (*8*–*10*), which indicates a LaMSA elastic storage system (*7*, *11*, *12*). Furthermore, our manipulation experiments refute the hypothesis of hydraulic pressure as the driving force (*21*–*25*). These findings, combined with morphological data and a bioinspired robotic model as proof of concept, provide compelling evidence for the hypothesis that the extensible mouthpart (prehensile labial mask) is driven by a dual-catapult mechanism.

Understanding complex biomechanical systems such as these not only highlights the evolutionary diversity of insects but also often leads to advances in the fields of bioinspired robotics and biomimetics. This mechanism is of special interest because it allows the synchronization of two catapult-driven joints, which are preloaded independently and to different degrees. This is advantageous for robotic applications where power modulation and thrust vector or directional control need to be combined. An example might be jumping robots that rely mostly on a single spring per leg (*31*) or several coupled springs (*32*, *33*). To achieve agile locomotion in more complex terrain, the robot needs to reorient itself (*34*) by either static (*35*) or dynamic (*36*, *37*) auxiliary control systems. The dual-catapult mechanism presented herein might be a way to improve controllability at the most basic level, thereby allowing for smaller and lighter control systems, and to increase the overall performance of power-modulated robotic systems.

RESULTS

General morphology and material composition

The extensible mouthpart (prehensile labial mask) is a highly modified apomorphic character (*19*, *20*), a structure unique to dragonflies and damselflies, used as a prey-capturing device (*18*). The overall structure consists of a distal segment 1 (prementum) and proximal segment 2 (postmentum), which are connected via a cubital-like hinge joint: The connecting joint [also referred to as prementum-postmentum joint (p-p joint)] allows uniaxial rotation of both segments relative to each other (Figs. 2, A to C, and 3) (*20*). The extensible mouthpart is connected to the head capsule ventrally via segment 2 by a membranous joint-like suspension, the head joint [also referred to as postmentum-head joint (p-h joint)], allowing uniaxial rotation of the entire extensible mouthpart relative to the head (Figs. 2, A to C, and 3) (*19*). The connecting joint consists of large membranous areas likely supplemented with the elastic protein resilin (*29*). For a detailed description of the morphology and/or material composition of the mouthparts of dragonflies, we refer to (*20*, *29*).

Introduction of the ILSDC

The proposed ILSDC mechanism for the protraction biomechanics of the extensible mouthpart of Odonata larvae consists of two connected, independently loaded catapults as the main driving force and activated simultaneously for the predatory strike of dragonfly larvae (Fig. 1B). Both independently spring-loaded (*7*, *11*) catapults generate the main power for the strike by storing elastic strain energy in resilin-dominated structures (Fig. 4, B and C) and likely in the surrounding cuticle [cf. (*38*, *39*)], enabling high-speed movement through rapid power conversion into kinetic energy. The first catapult moves the entire extensible mouthpart toward the prey, and the second catapult opens the connecting joint (p-p joint; Figs. 2 and 3) to unfold the extensible mouthpart (see movies S1 and S2). The system is locked by a complex latch mechanism consisting of three interlocking components (Fig. 4, D to J) to allow energy storage in spring-loaded systems (*11*). An active trigger is used for activating the two catapults to ensure the precise timing of the predatory strike (Figs. 3C and 4, H to J).

The presented ILSDC represents a biomechanically promising discovery because it differs considerably from already described catapult mechanisms. The mechanism forms a two-link kinematic chain, where each link can be preloaded and thereby controlled independently,

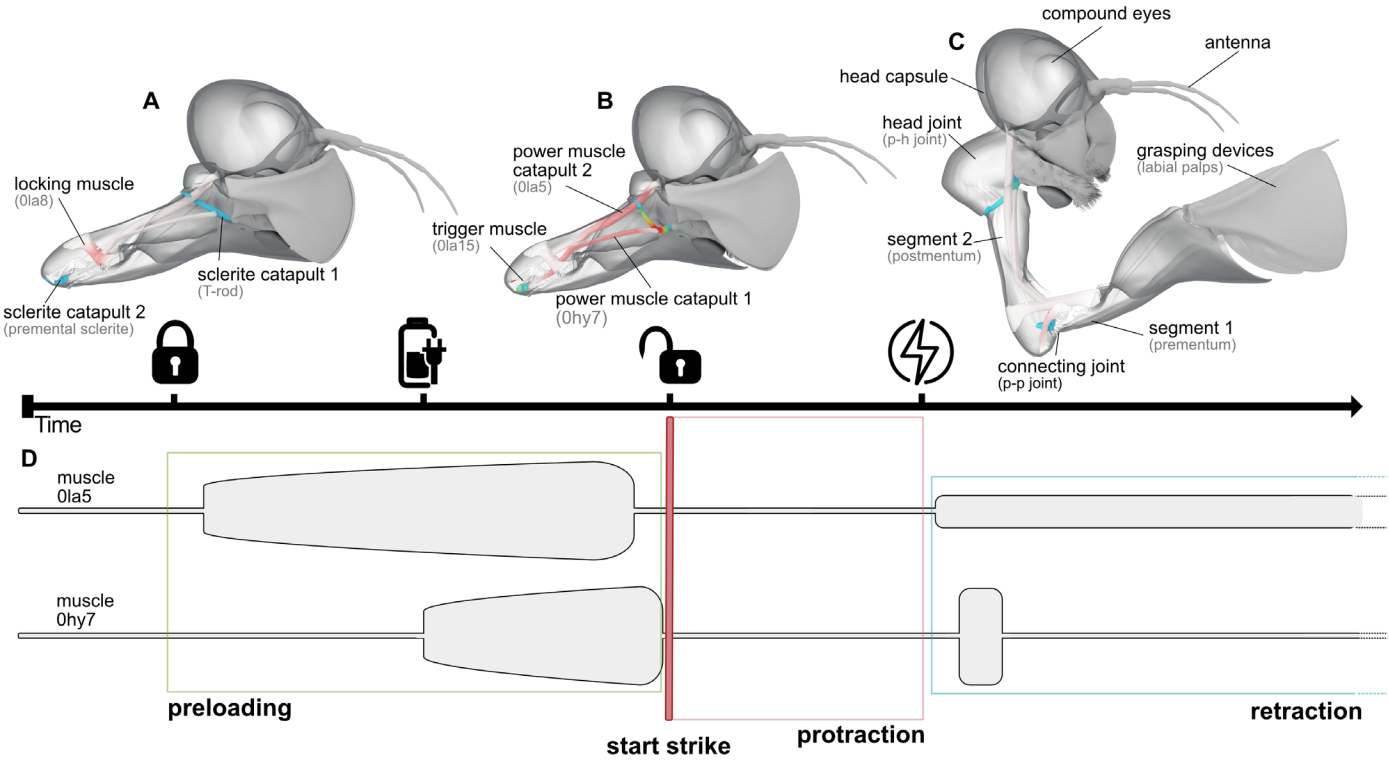

Fig. 2. Morphology of the extensible mouthpart and a simplified sequence of the predatory strike. The 3D visualizations were derived from μCT data of *Sympetrum* sp. (Odonata: Anisoptera). Color codes: gray muscles, relaxed; red muscles, contracted; blue sclerites, undeformed; red sclerites, deformed. (**A**) Preparation for the predatory strike, locking. (**B**) Preloading and triggering of the protraction. (**C**) Unlocking and protraction of the extensible mouthpart (prehensile labial mask). (**D**) Electrophysiology of the predatory strike, showing muscle activity of the power muscles (0la5 and 0hy7) during preloading, protraction, and retraction [modified after Tanaka and Hisada (*23*)].

whereas the system is mechanically synchronized by a single trigger. In contrast, the predatory strike of mantis shrimps (*5*) or the previously mentioned jump of froghoppers (*4*, *6*) does not allow for any adjustability between these segments because one catapult per leg moves the leg segments. The synchronization between the leg pairs is accomplished via a neuronal circuitry (*40*, *41*). Another possible example is the predatory and defensive strike of trap-jaw ants [cf. (*39*)]. The two catapult-powered mouthparts in trap-jaw ants (the two mandibles), each using one common lock and trigger, are separate structures but do not, however, represent a single kinematic chain as described for the Odonata larvae. The complex biomechanical processes of our ILSDC and all involved components are explained in a three-dimensional (3D) animation (movie S2), representing our biomechanical hypothesis. Furthermore, a detailed description of all involved structures can be found in the following.

The ILSDC in detail

The ILSDC consists of a two-link kinematic chain that can be subdivided into two independently loaded catapults mechanically synchronized with a single lock and trigger (Figs. 3 and 4). Catapult 2 unfolds segment 1 (prementum) and segment 2 (postmentum), and catapult 1 projects the entire prehensile labial mask (extensible mouthpart). The energy provided by the power muscle of catapult 1 (0hy7; Figs. 2 to 4) is stored in the spring of catapult 1 (T-rod): A small sclerite whose resilin-dominated material composition suggests flexible and resilient properties (Fig. 4, A and B, and fig. S4). The energy provided by the power muscle of catapult 2 (0la5) is stored in the spring of catapult 2 (premental sclerite; Figs. 2 to 4), which is also resilin dominated (Fig. 4, A and C, and fig. S4). After the latch system has been locked by the locking muscle (0la8; Fig. 3A), the power muscle of catapult 1 (0hy7) deflects the spring of catapult 1 (T-rod; force fm1 in Fig. 3B). Simultaneously, the power muscle of catapult 2 (0la5) deflects the spring of catapult 2 (premental sclerite) (force fm2 in Fig. 3B). To simulate the deformation of the sclerites, we used a muscle relaxant agent ($MgCl_2$) and a muscle contraction agent (KCl). We were able to show that muscle contraction induces a "loaded spring condition" (fig. S2, D and F), whereas muscle relaxation induces an "unloaded spring condition" (fig. S2 E and G; see also Materials and Methods). The fact that muscle contraction indeed deforms the sclerites corroborates our hypothesis that these structures are involved in the described catapult system and act as energy storage devices, likely in combination with the surrounding cuticle. This kind of energy-storing cuticle deformation is described for trap-jaw ants, for example, where the entire head is deformed to allow for their powerful mandibular strike [cf. (*39*)].

To lock the prehensile labial mask during preloading and to trigger a strike, we propose an active latch mechanism at the connecting joint (p-p joint). The latch mechanism is composed of (i) the locking groove [premental groove; cf. (*29*)], present on segment 1 (prementum;Fig. 4, D and G); (ii) the locking knob [postmental knob; cf. (*29*)], the counterpart to the groove on the corresponding area of segment 2 (postmentum); (iii) the locking wedge [p-p articulatory

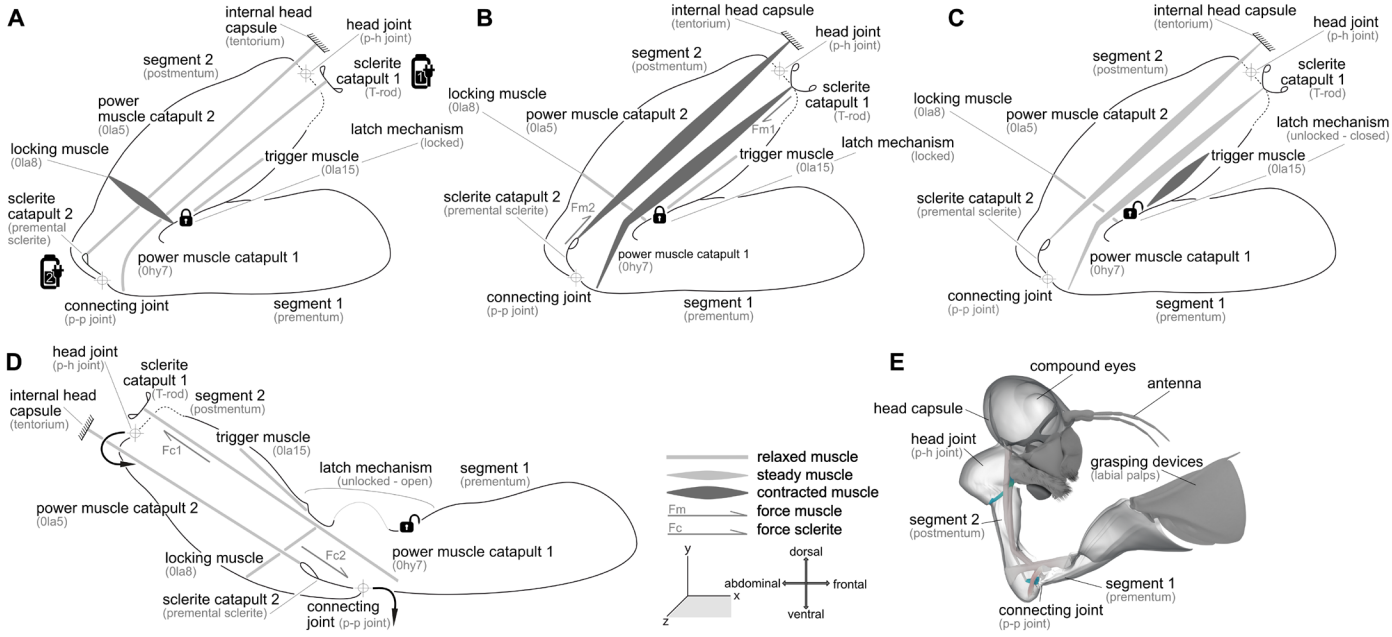

Fig. 3. Principle of movement of the extensible mouthpart and functioning of the ILSDC. (**A**) Locking: Contraction of the locking muscle (0la8) and closing the knob, groove, and wedge system (see Fig. 4D). (**B**) Preloading: Contraction of power muscle catapult 1 (0hy7) and deflection (fm1) of sclerite catapult 1 (T-rod) as well as contraction of power muscle catapult 2 (0la5) and deflection (fm2) of sclerite catapult 2 (premental sclerite). (**C**) Triggering: Contraction of the trigger muscle (0la15) and opening the knob, groove, and wedge system (see Fig. 4J). (**D**) Protraction: releasing the stored energy (fc1 and fc2) of sclerite catapult 1 (T-rod) and sclerite catapult 2 (premental sclerite) to project the extensible mouthpart (prehensile labial mask). (**E**) Morphology of the extensible mouthpart (prehensile labial mask); 3D visualization derived from μCT data of *Sympetrum* sp. (Odonata: Anisoptera).

plate; cf. (*29*)] within the connecting joints (p-p joint) articulation (Fig. 4, D and F); and (iv) the trigger muscle (0la15; Fig. 3A). (i) and (ii) form a clamp (Fig. 4, D and E). Before preloading starts, contraction of the locking muscle (0la8; Figs. 3A and 4A) provides the energy to actively push the knob over the groove (Fig. 3A and 4H), locking the system and enabling spring loading when needed. At this point, the locking knob (postmental knob) clamps behind the locking groove (premental groove), and the locking wedge (p-p articulatory plate) sits in between, locking these structures like a wedge (Figs. 3, A and B, and 4I). For a predatory strike, both catapults need to be triggered. Contraction of the trigger muscle (0la15; Fig. 3C) triggers the catapults by removing the wedge (p-p articulatory plate), forcing the locking groove (premental groove) and the locking knob (postmental knob) to slide apart (Figs. 3C and 4J).

The material composition of these cuticular structures supplement the locking function: The locking wedge (p-p articulatory plate) is divided into two parts with a resilin-dominated ridge at the divide, which allows the folding into a wedge. The locking groove (premental groove) is sclerotized and represents the slot for the locking knob (postmental knob). In turn, the knob serves as the clamp of the latch. It is composed of a sclerotized ridge at the contact area with the groove; the surrounding resilin-dominated areas allow for movability during locking and unlocking (Fig. 4, D to G). In the work of Büsse and Gorb (*29*), the material composition of these parts is described in more detail.

The release of segment 1 (prementum) changes the traction angles of the co-contracting power muscle catapult 1 (0hy7) and power muscle catapult 2 (0la5), causing power muscle catapult 2 [0la5; running above the pivot of rotation of the segment 2 (postmentum)] to lose tension rapidly. Therefore, the power muscle catapult 1 [0hy7; running below the pivot of rotation of the segment 2 (postmentum)], connected to the preloaded sclerite catapult 1 (T-rod), pulls segment 2 (postmentum) forward. Simultaneously, both the preloaded sclerite catapult 1 (T-rod) and the preloaded sclerite catapult 2 (premental sclerite) release the stored modulated power (force fc1 and fc2 in Fig. 3D), leading to a projection of the prehensile labial mask.

Performance of the ILSDC

The extensible mouthpart (prehensile labial mask) and the two compartments [segment 1 (prementum) and segment 2 (postmentum)] reach tangential velocities of Ø 0.5 and 0.7 m s^{-1}, angular velocities of Ø 71 and 73 rad s^{-1}, tangential acceleration of Ø 40 and 67 m s^{-2}, and peak angular acceleration of 5918 and 6674 rad m s^{-2}, respectively (Table 1 and figs. S1 and S5). For a typical strike, a power output of Ø 2233 and 2114 W kg^{-1} is necessary to achieve the mentioned performance. Here, we conservatively calculated the minimum power requirements (we neglect the drag of the system and therefore underestimate the power output); however, the calculated power output surpasses the power output of the fastest-contracting muscles known considerably (*8*–*10*). One of the most powerful muscles mentioned in literature is that of the blue breasted quail (*Coturnix chinensis*), reaching a maximum power output during takeoff of about 400 W kg^{-1} (*42*). The calculated power output for the catapult system powering the predatory strike of Odonata larvae is intermediate, between the lowest power output values for catapult systems using power modulation and the highest described in literature [cf. box 1 in (*12*)], for example, snow fleas (*43*) with 740 W kg^{-1} or flea beetles (*44*) with 714 W kg^{-1}, facing the most powerful systems like the jumps of froghoppers (*3*) with 3.6×10^4 W kg^{-1} or the most powerful predatory strike of mantis shrimps (*5*) with

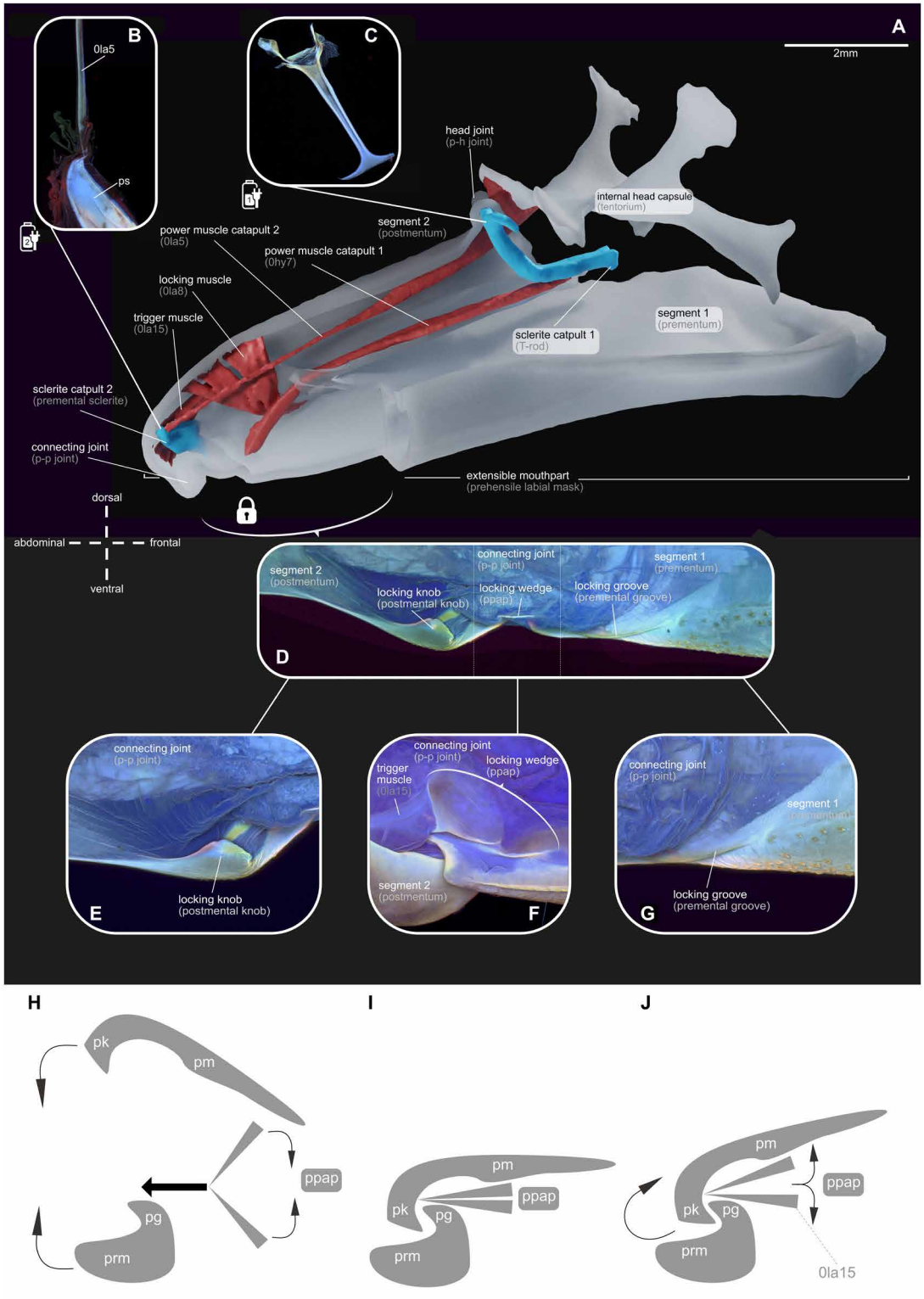

Fig. 4. Morphology and material composition of the power unit and locking mechanism of the ILSDC in *Anax* sp. (Odonata: Anisoptera). (**A**) Extensible mouthpart (prehensile labial mask), 3D visualization derived from μCT data. (**B** to **G**) CLSM maximum intensity projection. Autofluorescence indicates the material composition of the cuticle: red, sclerotized; green, chitinous; and blue, resilin dominated (*28*). (B) Sclerite catapult 1 (T-rod). (C) Sclerite catapult 2 (premental sclerite) and power muscle catapult 2 (0la5). (D) Locking mechanism of the labial mask, dorsal view. (E) Locking groove (premental groove), detail, dorsal view. (F) Locking wedge (prementum-postmentum articulatory plate), detail, lateral view. (G) Locking knob (postmental knob), detail, median view. (**H** to **J**) Principle of the locking/unlocking process. (H) Locking. (I) Locked. (J) Unlocking. pg, premental groove (locking groove); pk, postmental knob (locking knob); pm, postmentum (segment 2); ppap, prementum-postmentum articulatory plate (locking wedge); prm, prementum (segment 1).

Table 1. Key characteristics of the performance of the predatory strike. Angle, maximum opening angle from resting position for both prementum and postmentum in (°); ω, maximum angular velocity of both the pre- and postmentum during protraction in radians per second; *v*, maximum tangential velocity at the distal tip of the prementum/postmentum, calculated from angular velocity; α, maximum angular acceleration calculated as first derivative from angular velocity in rad/s^2; a_T, tangential acceleration at the distal tip of prementum/postmentum, calculated from angular acceleration in m/s^2 and g; *N*, number of biological replicates.

	Segment 1 (prementum)		Segment 2 (postmentum)		
	Mean	**SD**	**Mean**	**SD**	***N***
Angle (°)	79	11	126	5	3
ω (rad/s)	72.54	33.32	71.42	26.89	5
v (m/s)	0.73	0.33	0.49	0.18	5
α (rad/s^2)	6673.50	3697.30	5917.69	3046.10	5
a_T (m/s^2)	66.74	36.97	40.24	20.71	5
a_T (g)	6.80	3.77	4.10	2.11	5
P (W/kg)	2113.53	2535.46	2232.81	2560.41	5

Table 2. Key characteristics of the performance the robotic model. Angle, maximum opening angle from resting position for both segment 1 (resembling the prementum) and segment 2 (resembling the postmentum) in (°); ω, maximum angular velocity of each segment during protraction in radians per second; *v*, maximum tangential velocity at the distal tip of each segment, calculated from angular velocity; *N*, number of recorded strikes.

	Segment 1 (prementum)		Segment 2 (postmentum)		
	Mean	**SD**	**Mean**	**SD**	***N***
Angle (°)	114.8	4.5	61.6	8.8	12
ω (rad/s)	26.74	5.02	12.36	2.39	12
v (m/s)	4.41	0.83	1.92	0.37	12
α (rad/s^2)	1471.75	524.61	453.47	244.95	12
a_T (m/s^2)	323.79	115.41	70.29	37.97	12
a_T (g)	33.01	11.76	7.16	3.87	12
P (W)	48.56	1.00	29.67	1.23	12

4.7×10^5 W kg^{-1}. This confirms that the predatory strike of Odonata larvae is indeed power modulated.

Manipulation experiments and support of the hypothesis

As mentioned before, the power output of the system surpasses the maximum power of a muscle, as already suggested in (*24*). However, previous investigations indicated that the driving power for the protraction of the extensible mouthpart (prehensile labial mask) is provided by hydraulic pressure (*21*–*25*). In our high-speed video experiments, we showed that *Anax* larvae (n = 5) eject a water jet from the rectal chamber (jet propulsion) during the prey-capturing process (see movie S3, part A). The simultaneity of predatory strike and jet propulsion is most likely a mechanism to counter the recoil, which originates from the antagonistic force of quickly accelerating the rather large extensible mouthpart (*45*). This observation is further supported by high-speed video recordings of *Sympetrum* larvae, where the larvae show no jet propulsion but a distinct recoil during the prey-capturing process is observed (see movie S3, part B). Larvae of this taxon are partially burrowed in the soil during hunting (*18*), so jet propulsion seems to not be required for recoil prevention. Furthermore, our observations show dragonflies using jet propulsion for movement toward prey and performing a predatory strike almost simultaneously. These observations are supported by similar findings for other anisopteran species (*46*). Jet propulsion and propelling the extensible mouthpart cannot be controlled by the same mechanism, especially because the predatory strike needs a closed abdomen (anal valve) and jet propulsion needs an open one (*21*). However, the simultaneity of these processes may explain the peaks in the hydraulic measurements during the prey-capturing process in earlier investigations (*22*–*26*), and therefore, it is likely that the involvement of hydraulic pressure in the protraction of the extensible mouthpart is misinterpreted.

Furthermore, the study of Tanaka and Hisada (*24*), especially the included electrophysiology, impressively showed that the only muscles capable of moving segment 1 (prementum) and 2 (postmentum), the power muscle catapult 2 [0la5; extensor (*24*)] and power muscle catapult 1 [0hy7; flexor (*24*)], are not active during the protraction of the extensible mouthpart (Fig. 2D). Their experiments highly support our findings that (i) both power muscles are active before the starting point of the predatory strike; (ii) both muscles are inactive during the main power output of the system, the protraction; and (iii) muscles are active again during the retraction of the extensible mouthpart (Fig. 2D) (*24*). Moreover, their muscle dissection experiments (*24*) showed the importance of the extensible mouthpart's musculature. Dissection of either power muscle catapult 1 (0hy7) or the power muscle of catapult 2 (0la5) causes abnormal strike movements. Especially after the dissection of the power muscle of catapult 1 (0hy7), the head joint (p-h joint) remains immobile, whereas the connecting joint (p-p joint) opens rapidly and the extensible mouthpart hits the ground (*24*). In this case, the power muscle catapult 1 (0hy7) is unable to preload the spring of catapult 1 (T-rod), causing the abnormal strike behavior: This, however, does not affect catapult 2. In addition, we performed manipulation experiments, using the physiological effect of $MgCl_2$ as muscle relaxant agent (*47*) to manipulate the abdominal muscles of the rectal chamber (*26*, *27*) to prevent the generation of hydraulic pressure either for jet propulsion or for the protraction of the extensible mouthpart (*21*–*25*). After injecting $MgCl_2$ into parts of the abdominal muscles related to the rectal chamber, *Anax* larvae (n = 5) were able to perform a predatory strike but could not use jet propulsion as an escape mechanism in response to an external stimulus (see movie S4). As a control, unmanipulated *Anax* larvae (n = 5) showed jet propulsion in direct response to an external stimulus (see movie S4). The findings of these experiments strongly corroborate our hypothesis that the driving power for the protraction of the extensible mouthpart is generated by an ILSDC.

Robotic model

To test whether the hypothesized interplay of muscles, springs and locks can actually generate a predatory strike–like motion, we used our detailed morphological findings to create a robotic model of the extensible mouthpart (prehensile labial mask; Fig. 5). The

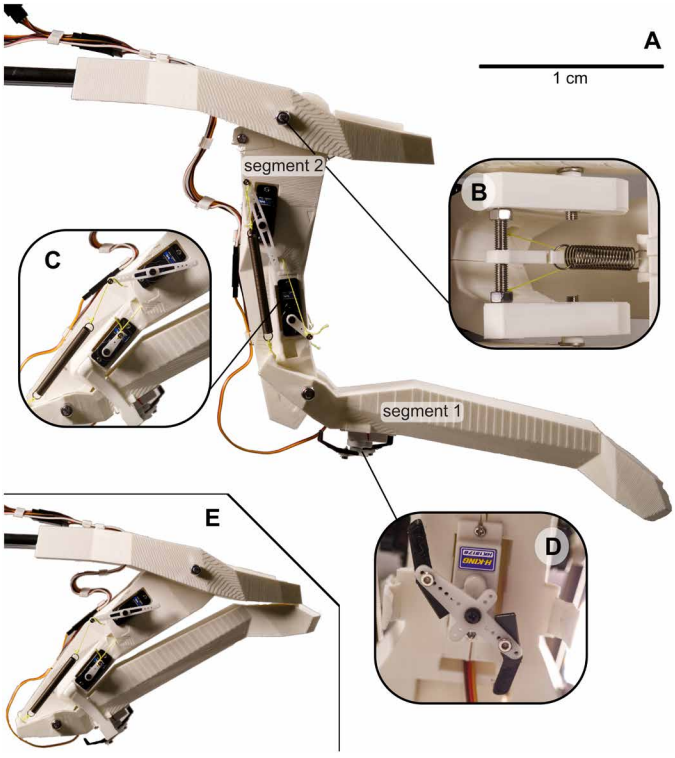

Fig. 5. Proof of concept of robotic extensible mouthpart, 3D printed. (**A**) Open. (**B**) Artificial spring catapult 1. (**C**) Artificial spring catapult 2 and artificial muscles (servo motors). (**D**) Artificial lock (servo motor). (**E**) Closed.

micro–computed tomography (μCT) data were used to ascertain general proportions and match the axes of rotation of both head joint (p-h joint) and connecting joint (p-p joint). Muscle movement was imitated by servomotors with matched traction angles. The energy-storing sclerites were imitated by steel tension springs (see Material and Methods). Using this setup, on the basis of the described morphology and hypothesized mechanical configuration, we show that the artificial extensible mouthpart moves in a comparable way to the real predatory strike of a dragonfly larva (see movie S5). This proof of concept intriguingly underlines our hypothesis. To test the hypothesis of power modulation, we performed 12 strikes with springs and another 10 with a direct coupling between the motors and segments and then calculated the power output of both configurations (Table 2). As the servomotors provide a peak power of 1.9 W, 3.8 W is available to drive each segment (two servos are used per segment). The results of our analysis show that 29.7 W are necessary to achieve the observed angular speed and acceleration at segment 2 (the postmentum) and 48.6 W at segment 1 (the prementum). These values exceed the peak power of the servos, verifying that our system provides power modulation. Although previous studies already used multisprings in robotic designs (*32*, *48*), these designs used coupled springs primarily to provide more energy for the jump (*32*). However, the configuration of motors and springs in the extensible mouthpart of Odonata larvae (as well as our robotic model) allows for independent preloading of both springs. Therefore, the acceleration of each segment can be controlled separately. Odonata larvae likely make use of this differential preloading to adjust for the height and distance of a prey item, a capability that has been observed previously (*21*, *49*). We tested this capability in our model as well, by using three different preloading states [A: full preloading of catapult 1 (100%), half preloading of catapult 2 (50%); B: full preloading of both catapults 100%/100%; and C: half preloading of catapult 1 (50%), full preloading of catapult 2 (100%)]. We recorded six strikes in each state and tracked the tip of segment 2. The results are shown in Fig. 6, and an overlay of two exemplary strikes (condition A and condition C) are shown in movie S5. Depending on the preloading conditions, the trajectories of the prementum are distinctly clustered, suggesting that differential preloading could be used to control such a robotic system. However, to investigate the relationship between targeting, preloading, and triggering in the robotic model, further research and more sophisticated models are necessary, but the observed power modulation and adjustability shows that this might be a promising configuration for future designs in bioinspired robotics.

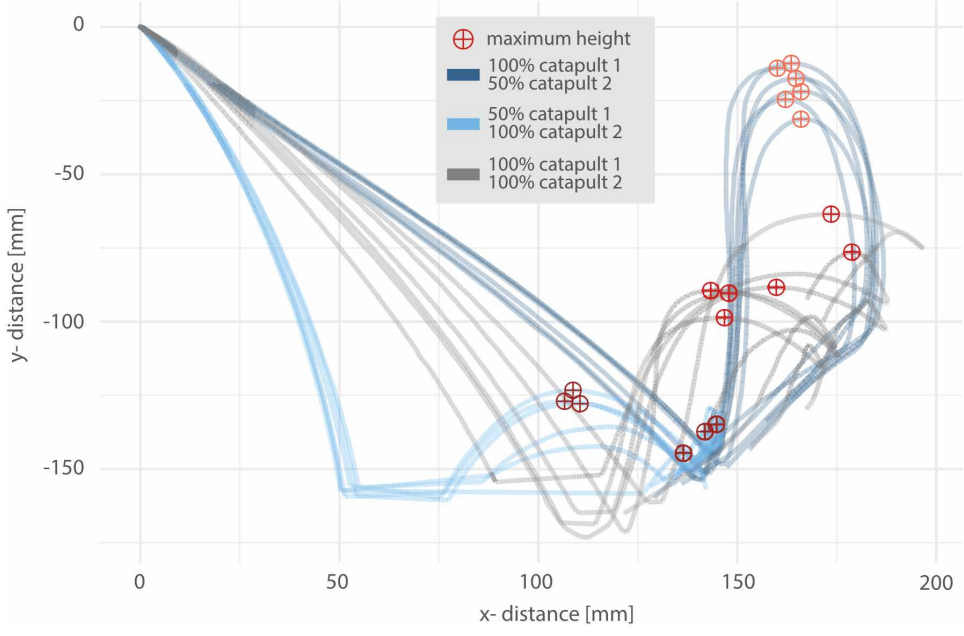

Fig. 6. Independent preloading trajectories of the tip of segment 1 depending on the preloading of both catapults. Trajectories are mapped in 2D space with the tip in the resting position as origin of the coordinate system. The maximum strike height (achieved after both segments unfolded) was used as a metric to compare the trajectories. Six strikes ($n = 6$) of three different preloading conditions were recorded (full preloading of catapult 1, half preloading of catapult 2; full preloading of both catapults; half preloading of catapult 1, full preloading of catapult 2).

CONCLUSIONS

We have shown that the power output of the extensible mouthpart exceeds the maximum power of a muscle, therefore making a purely muscle-driven

movement impossible. The previously proposed hydraulic hypothesis as a driving force for the predatory strike was likely a misinterpretation and is not able to power the predatory strike, and the present morphology of the extensible mouthpart (prehensile labial mask) represents two interconnected catapult systems. The question of whether the energy for this high-speed movement is solely stored in the described resilin-dominated sclerites, or whether parts of the surrounding cuticle are involved as well, requires further research. However, this does not change the functional principle that we described here. Our proof of concept using a robotic model shows the functionality of the proposed mechanism. Thus, our study elucidates the predatory strike of dragonfly larvae by proposing an ILSDC mechanism, while also highlighting the role of the cuticle as a complex composite material, enabling structural integrity and energy storage as one of the main components required for these movements. By implementing two catapults, each driving one joint of the kinematic chain, which are triggered together but can be preloaded independently, this mechanism is potentially capable of higher targeting accuracy than other catapult systems. Implication of such a mechanism allows for thrust vector control in jumping robots, enhancing the maneuverability and agility of such systems. This makes the prehensile labial mask (extensible mouthpart) an intriguing model for further research concerning catapults in biology and bioinspired robotics.

MATERIALS AND METHODS

Animals

Specimens of *Anax* sp. (Anisoptera: Aeshnidae) and *Sympetrum* sp. (Anisoptera: Libellulidae) were collected in Kiel (Germany) in 2016 and 2017 with permission from the Landesamt für Landwirtschaft, Umwelt und ländliche Räume Schleswig-Holstein.

Study design

We designed the study to refute the previous hypothesis of the driving force of the predatory strike of dragonfly larvae and describe the morphology and biomechanics of the ILSDC system. To reach this goal, we combined biological manipulation experiments, high-speed videography, µCT, confocal laser scanning microscopy (CLSM), and 3D printing. The sample size varies because of investigation method and is stated in every paragraph. For the morphological investigations, three specimens per treatment were used; for the kinematics and manipulation experiments, five specimens were used.

Micro–computed tomography

Before µCT analysis, specimens ($n = 3$ per treatment) were fixed for high tissue preservation in alcoholic Bouin solution (Duboscq-Brasil). We used three different treatments before the tissue preservation: (i) for muscle relaxation, prefixation in magnesium chloride ($MgCl_2$); (ii) for muscle contraction, prefixation in potassium chloride (KCl); and (iii) no prefixation. To guarantee that the fixation with KCL and $MgCL_2$ does not cause artifacts, we incubated test samples ($n = 3$ per structure) for 48 hours and measured their dimensions using an optical 3D measuring microscope (VR-3000 series, KEYENCE, Osaka, Japan; fig. S3). Before scanning, the samples were dehydrated in an ascending ethanol series and critical-point dried (Quorum E3000; Quorum Tech Ltd., Laughton, UK). For µCT, the critical-point dried samples were mounted on a device-specific specimen holder and scanned (SkyScan 1172; Bruker micro-CT, Kontich, Belgium) with high-resolution settings (40 kV, 250 µA, and 0.25° rotation steps, performing a 360° scan). Segmentation and processing of the µCT data were carried out with Amira 6.0.1 (FEI SAS, Lyon, France). The segmented data were exported as Wavefront ".obj" files for further processing. For 3D visualization, textures and material shaders for rendering were applied using the open-source 3D creation suite Blender (Blender Foundation, Amsterdam, Netherlands; www.blender.org). To visualize our hypothesis of the predatory strike, an armature rig was applied to a CT data–based, retopologized 3D model, and keyframe animation was performed using the high-speed videos as references for correct positioning, angles, and timing of the animation. Clips were created using the integrated "Cycles" rendering engine with a resolution of 1920 pixels by 1080 pixels at 25 frames per second (fps). Animation sequences were saved as "Cineon" image stacks, and the final clip was edited in Adobe Premiere Pro CS6 (Adobe Systems Software, San José, CA, USA). Additional 2D animations were created in Adobe After Effects CS6 (Adobe Systems Software, San José, CA, USA).

Confocal laser scanning microscopy

All specimens used for CLSM were freshly frozen and stored at −70°C. The samples were washed in ethanol (100%), and dirt particles were removed using ultrasonic cleaning (SONOREX RK52; Bandelin, Berlin, Germany). The dissected parts were embedded in glycerin (99.99%) on a glass slide and covered with a high-precision cover slip (Carl Zeiss Microscopy, Jena, Germany) before scanning. For visualization, a Zeiss LSM 700 (Carl Zeiss Microscopy, Jena, Germany) was used with the wavelengths of 405, 488, 555, and 639 nm and the emission filters BP420-480, LP490, LP560, and LP640 nm. Maximum intensity projections were created using ZEN 2008 software (www.zeiss.de/mikroskopie). For more information on using CLSM to determine the material properties of the insect cuticle, refer to Michels and Gorb (*50*) or Büsse and Gorb (*29*). All images obtained via µCT and CLSM were subsequently processed and combined into figure plates using Affinity Photo and Affinity Design (www.affinity.serif.com).

Toluidine blue staining

As secondary resilin verification, we used a toluidine blue staining (*14*, *50*–*53*). The structures (T-rod and premental sclerite) were incubated with 0.1 to 0.5% toluidine blue (in an aqueous solution of 1% sodium tetraborate) for 30 to 60 s and destained using glycerin for 48 hours (see fig. S4). Samples were subsequently analyzed using an optical 3D measuring microscope (VR-3000 series, KEYENCE, Osaka, Japan) to detect the bluish stain of resilin-containing structures.

High-speed video recordings

For the high-speed video recordings of the prey-capturing process, we used a Photron FASTCAM SA1.1 (model 675K-M1; Photron, Pfullingen, Germany) equipped with a 105-mm/1:2.8 macro lens (Sigma, Tokyo, Japan) mounted on a Manfrotto-055 tripod with a Manfrotto-410 geared head (Manfrotto, Spa, Italy) and two Dedocool COOLT3 light sources (Dedotec, Berikon, Switzerland; settings, 5400 fps; exposure time, 1 per frame; trigger mode, end; and resolution: 1024 pixels by 1024 pixels). The footage was saved as 16-bit TIFF image stacks. Predatory strikes of five specimens of each *Anax* sp. and *Sympetrum* sp. were recorded, with two strikes per individual. Chironomid larvae were manually presented as prey items.

Motion tracking

Frame-by-frame data on the position of the prehensile labial mask were obtained from five individuals of *Anax* sp. using the workflow described by Koehnsen *et al.* (*54*). From tracking coordinates, the angle between head capsule and postmentum, as well as prementum and postmentum, was calculated for every frame. Angular velocity was calculated at every fourth frame, and data were smoothed using an 11th-order polynomial (polynomial regression using R; see also fig. S1B). Angular acceleration was calculated as first-order derivative of the obtained curve. Peak velocity and acceleration were obtained from local maxima of the respective curves. Tangential velocity/acceleration at the tip of the prementum/postmentum was calculated from angular velocity/acceleration with the radius r being the average distance from the pivot point to the tip of the respective structure based on all study animals used (n = 5). All calculations were performed using the open-source statistical computation software R Studio (version 3.3.1; The R Foundation for Statistical Computing, Vienna, Austria).

Terminology

We used the term dragonfly(ies) for Odonata (dragonflies + damselflies) for the sake of simplicity. Morphological terminology was used after Büsse *et al.* (*20*) and Büsse and Gorb (*29*). Furthermore, we decided to use the term power modulation rather than power amplification. The latter is widespread within the biomechanics literature, yet it is misleading. The total energy of a system is conserved over time (first law of thermodynamics). The power (and concordantly energy) output of a closed system can therefore not be amplified by means within the system, which the term power amplification suggests. Instead, the power output is modulated (*36*). Energy is stored and later released, leading to an increased peak power output. For more information on the topic, we suggest the work by Haldane *et al.* (*36*).

Power output calculations

The power output calculation can be found in the Supplementary Materials.

Manipulation experiments

For the manipulation experiments, we injected 2 to 4 ml of a 20 mM solution of magnesium chloride ($MgCl_2$) as a muscle relaxant agent (*47*) into the abdominal dorsoventral muscles of *Anax* sp. larvae (n = 5). After 2 to 5 min, the injected dorsoventral musculature was relaxed, and the specimens were not able to produce the necessary hydraulic pressure for jet propulsion (in response to an external stimulus). Chironomid larvae (Insecta: Diptera) were manually presented as prey items. After a successful predatory strike, the larvae were given an external stimulus to trigger an escape reaction. We scored the ability to use jet propulsion as an escape mechanism after a successful predatory strike in manipulated and unmanipulated specimens.

Robotic model (proof of concept)

We constructed an artificial model as proof of concept for the hypothesized catapult-driven prehensile labial mask. A 3D model was designed using the 3D creation suite Blender (v2.79, Blender Foundation, Netherlands; www.blender.org). Relative proportions, axes of rotation, and angles of traction were derived from CT data and high-speed videography. Individual parts were exported as ".stl" files and printed on a Prusa i3 Mk2S FDM 3D printer (Prusa Research s.r.o., Prague, Czech Republic) using polylactic acid filament (Prusa Research s.r.o., Prague, Czech Republic). Steel tension springs (one 9.1 mm–by–27.4 mm–by–1 mm spring at the p-h catapult and two 5.7 mm–by–59.2 mm–by–0.06 mm springs at the p-p catapult) serve as energy storage devices. Each catapult is preloaded using two Turnigy MX-M801 servo motors (HexTronics Ltd., Kowloon Bay, Hong Kong) with a peak power of 1.9 W, a maximum moment of 0.196 N·m, and a rotational speed of max 9.52 rad/s. The latch mechanism is triggered using a HobbyKing HK15178 servomotor (HexTronics Ltd., Kowloon Bay, Hong Kong). Motors are controlled by an Arduino Uno R2 Board (Arduino.cc) using custom code. The entire system is powered with a 5-V 600-mA power supply unit (ELEGOO Power MB V2, ELEGOO Inc., Shenzhen, China).

High-speed video footage of the artificial labial mask was captured at 1000 fps at a resolution of 1280 pixels by 1024 pixels using an Olympus i-SPEED 3 high-speed camera (iX Cameras, Rochford, Essex, UK) equipped with a Sigma Compact Hyperzoom 28 to 200 mm/1:3.5 to 5.6 macro lens (Sigma, Tokyo, Japan). Data were saved in the AVI codec and edited using Adobe Premiere CS6 (Adobe Systems Software, San José, CA, USA). To analyze the dynamic properties of the mechanism, 12 strikes were recorded using a Sony RX0 II camera (Sony Corporation, Tokyo, Japan) modified with a Back-Bone Ribcage RX0 II adapter (Back-Bone Gear Inc., Kanata, Canada) to accommodate a Samyang 100-mm F2.8 macro lens (Samyang Optics, Masan, South Korea). Footage was captured at 1000 fps with a resolution of 1920 pixels by 1080 pixels and saved using the H264 codec. Footage was tracked, and peak power was calculated as stated previously for the animal footage.

SUPPLEMENTARY MATERIALS

robotics.sciencemag.org/cgi/content/full/6/50/eabc8170/DC1
Power output calculations
Fig. S1. Kinematics of the predatory strike based on motion-tracking data.
Fig. S2. Deformation of sclerites.
Fig. S3. Artifacts control.
Fig. S4. Toluidine blue staining.
Fig. S5. Schemes of the predatory strike of Odonata larvae (for power output calculation).
Movie S1. *Anax* sp. (Odonata: Anisoptera), high-speed videography of the predatory strike, 5400 fps.
Movie S2. Fictive 3D animation of the predatory strike, based on CT data.
Movie S3. *Anax* sp. (Odonata: Anisoptera), high-speed videography of recoil prevention, 5400 fps.
Movie S4. *Anax* sp. (Odonata: Anisoptera), videography of the manipulation experiments.
Movie S5. Bioinspired robotic model, videography of the proof of the concept and loading experiments.

REFERENCES AND NOTES

1. R. Dawkins, J. R. Krebs, Arms races between and within species. *Proc. R. Soc. Lond. B* **205**, 489–511 (1979).
2. H. C. Bennet-Clark, The energetics of the jump of the locust *Schistocerca gregaria*. *J. Exp. Biol.* **63**, 53–83 (1975).
3. M. Burrows, Biomechanics: Froghopper insects leap to new heights. *Nature* **424**, 509 (2003).
4. S. N. Gorb, The jumping mechanism of cicada *Cercopis vulnerata* (Auchenorrhyncha, Cercopidae): Skeleton–muscle organisation, frictional surfaces, and inverse-kinematic model of leg movements. *Arthropod Struc. Dev.* **33**, 201–220 (2004).
5. S. N. Patek, W. L. Korff, R. L. Caldwell, Biomechanics: Deadly strike mechanism of a mantis shrimp. *Nature* **428**, 819–820 (2004).
6. M. Burrows, S. R. Shaw, G. P. Sutton, Resilin and chitinous cuticle form a composite structure for energy storage in jumping by froghopper insects. *BMC Biol.* **6**, 41 (2008).
7. M. Ilton, M. S. Bhamla, X. Ma, S. M. Cox, L. L. Fitchett, Y. Kim, J.-S. Koh, D. Krishnamurthy, C.-Y. Kuo, F. Z. Temel, A. J. Crosby, M. Prakash, G. P. Sutton, R. J. Wood, E. Azizi, S. Bergbreiter, S. N. Patek, The principles of cascading power limits in small, fast biological and engineered systems. *Science* **360**, eaao1082 (2018).

8. R. K. Josephson, Contraction dynamics and power output of skeletal muscle. *Annu. Rev. Physiol.* **55**, 527–546 (1993).
9. R. M. Alexander, H. C. Bennet-Clark, Storage of elastic strain energy in muscle and other tissues. *Nature* **265**, 114–117 (1977).
10. R. M. Alexander, Tendon elasticity and muscle function. *Comp. Biochem. Phys. A Mol. Integr. Physiol.* **133**, 1001–1011 (2002).
11. W. Gronenberg, Fast actions in small animals: Springs and click mechanisms. *J. Comp. Physiol. A* **178**, 727–734 (1996).
12. S. J. Longo, S. M. Cox, E. Azizi, M. Ilton, J. P. Olberding, R. S. Pierre, S. N. Patek, Beyond power amplification: Latch-mediated spring actuation is an emerging framework for the study of diverse elastic systems. *J. Exp. Biol.* **222**, jeb197889 (2019).
13. J. Michels, E. Appel, S. N. Gorb, Functional diversity of resilin in Arthropoda. *Beilstein J. Nanotechnol.* **7**, 1241–1259 (2016).
14. T. Weis-Fogh, Resilin. A rubber-like protein in insect cuticle. *J. Exp. Biol.* **37**, 889–907 (1960).
15. R. E. Lyons, D. C. C. Wong, M. Kim, N. Lekieffre, M. G. Huson, T. Vuocolo, D. J. Merritt, K. M. Nairn, D. M. Dudek, M. L. Colgrave, C. M. Elvin, Molecular and functional characterisation of resilin across three insect orders. *Insect Biochem. Mol. Biol.* **41**, 881–890 (2011).
16. T. Weis-Fogh, Molecular interpretation of the elasticity of resilin, a rubber-like protein. *J. Mol. Biol.* **3**, 648–667 (1961).
17. C. M. Elvin, A. G. Carr, M. G. Huson, J. M. Maxwell, R. D. Pearson, T. Vuocolo, N. E. Liyou, D. C. C. Wong, D. J. Merritt, N. E. Dixon, Synthesis and properties of crosslinked recombinant pro-resilin. *Nature* **437**, 999–1002 (2005).
18. P. S. Corbet, *Dragonflies: Behavior and Ecology of Odonata* (Cornell Univ. Press, 1999).
19. R. E. Snodgrass, The dragonfly larva. *Smith. Misc. Coll.* **12**, 38 (1954).
20. S. Büsse, T. Hörnschemeyer, S. N. Gorb, The head morphology of *Pyrrhosoma nymphula* larvae (Odonata: Zygoptera) focusing on functional aspects of the mouthparts. *Front. Zool.* **14**, 25 (2017).
21. G. Pritchard, Prey capture by dragonfly larvae (Odonata; Anisoptera). *Canad. J. Zool.* **43**, 271–289 (1965).
22. J. Olesen, The hydraulic mechanism of labial extension and jet propulsion in dragonfly nymphs. *J. Comp. Physiol.* **81**, 53–55 (1972).
23. J. Olesen, Prey-capture in dragonfly nymphs (Odonata; Insecta): Labial protraction by means of a multipurpose abdominal pump. *Vid. Medd. Dan. Naturalist. Foren.* **141**, 81–96 (1979).
24. Y. Tanaka, M. Hisada, The hydraulic mechanism of the predatory strike in dragonfly larvae. *J. Exp. Biol.* **88**, 1–20 (1980).
25. D. A. Parry, Labial extension in the dragonfly larva *Anax imperator*. *J. Exp. Biol.* **107**, 495–499 (1983).
26. P. J. Mill, R. S. Pickard, Anal valve movement and normal ventilation in *Aeshnid* dragonfly larvae. *J. Exp. Biol.* **56**, 537–543 (1972).
27. P. J. Mill, R. S. Pickard, Jet-propulsion in anisopteran dragonfly larvae. *J. Comp. Physiol.* **97**, 320–338 (1975).
28. K. S. Cole, D. L. Gilbert, Jet propulsion of squid. *Biol. Bull.* **138**, 245–246 (1970).
29. S. Büsse, S. N. Gorb, Material composition of the mouthpart cuticle in a damselfly larva (Insecta: Odonata) and its biomechanical significance. *Royal Soc. Open Sci.* **5**, 172117 (2018).
30. A. Blanke, S. Büsse, R. Machida, Coding characters from different life stages for phylogenetic reconstruction: A case study on dragonfly adults and larvae, including a description of the larval head anatomy of *Epiophlebia superstes* (Odonata: Epiophlebiidae). *Zool. J. Linn. Soc.* **174**, 718–732 (2015).
31. C. Zhang, W. Zou, L. Ma, Z. Wang, Biologically inspired jumping robots: A comprehensive review. *Rob. Auton. Syst.* **124**, 103362 (2020).
32. L. Wang, F. Meng, H. Liu, X. Fan, R. Sato, A. Ming, Q. Huang, Design and implementation of jumping robot with multi-springs based on the coupling of polyarticular. *Int. Conf. Robot. Biomim.* **2018**, 287–292 (2018).
33. M. A. Woodward, M. Sitti, Multimo-bat: A biologically inspired integrated jumping–gliding robot. *Int. J. Robotics Res.* **33**, 1511–1529 (2014).
34. A. J. Ijspeert, Biorobotics: Using robots to emulate and investigate agile locomotion. *Science* **346**, 27–29 (2014).
35. M. Kovač, M. Schlegel, J. C. Zufferey, D. Floreano, Steerable miniature jumping robot. *Auton. Robots* **28**, 295–306 (2010).
36. D. W. Haldane, M. M. Plecnik, J. K. Yimand, R. S. Fearing, Robotic vertical jumping agility via series-elastic power modulation. *Sci. Robot.* **1**, eaag2048 (2016).
37. D. W. Haldane, J. K. Yim, R. S. Fearing, Repetitive extreme-acceleration (14-g) spatial jumping with Salto-1P. *IEEE Int. Conf. Intell. Robot. Syst.* **2017**, 3345–3351 (2017).
38. M. Burrows, G. P. Sutton, Locusts use a composite of resilin and hard cuticle as an energy store for jumping and kicking. *J. Exp. Biol.* **215**, 3501–3512 (2012).
39. F. J. Larabee, W. Gronenberg, A. V. Suarez, Performance, morphology and control of power-amplified mandibles in the trap-jaw ant *Myrmoteras* (Hymenoptera: Formicidae). *J. Exp. Biol.* **220**, 3062–3071 (2017).
40. M. Burrows, Neural control and coordination of jumping in froghopper insects. *J. Neurophysiol.* **97**, 320–330 (2007).
41. M. Burrows, The mechanics and neural control of the prey capture strike in the mantid shrimps *Squilla* and *Hemisquilla*. *Z. Vergl. Physiologie* **62**, 361–381 (1969).
42. G. N. Askew, R. L. Marsh, Muscle designed for maximum short-term power output: Quail flight muscle. *J. Exp.Biol.* **205**, 2153–2160 (2002).
43. M. Burrows, Jumping mechanisms and performance of snow fleas (Mecoptera, Boreidae). *J. Exp.Biol.* **214**, 2362–2374 (2011).
44. K. Nadein, O. Betz, Jumping mechanisms and performance in beetles. I. Flea beetles (Coleoptera: Chrysomelidae: Alticini). *J. Exp.Biol.* **219**, 2015–2027 (2016).
45. S. Vogel, *Life in Moving Fluids* (Princeton Univ. Press, 1994).
46. R. J. Rowe, Predatory versatility in a larval dragonfly, *Hemianax papuensis* (Odonata: Aeshnidae). *J. Zool. Lond.* **221**, 193–207 (1987).
47. S. Ebaschi, Calcium binding activity of vesicular relaxing factor. *J. Biochem.* **50**, 236–244 (1961).
48. E. Kazama, R. Sato, I. Miyamoto, A. Ming, Development of a small quadruped robot with bi-articular muscle-tendon complex. *Int. Conf. Robot. Biomimetics* **2015**, 1059–1064 (2015).
49. E. Quenta-Herrera, J. Casas, O. Dangles, S. Pincebourde, Temperature effects on ballistic prey capture by a dragonfly larva. *Ecol. Evol.* **8**, 4303–4311 (2018).
50. J. Michels, S. N. Gorb, Detailed three-dimensional visualization of resilin in the exoskeleton of arthropods using confocal laser scanning microscopy. *J. Microsc.* **245**, 1–16 (2012).
51. D. Young, H. Bennet-Clark, The role of the tymbal in cicada sound production. *J. Exp.Biol.* **198**, 1001–1019 (1995).
52. E. Appel, L. Heepe, C.-P. Lin, S. N. Gorb, Ultrastructure of dragonfly wing veins: Composite structure of fibrous material supplemented by resilin. *J. Anat.* **227**, 561–582 (2015).
53. I. Siwanowicz, M. Burrows, Three dimensional reconstruction of energy stores for jumping in planthoppers and froghoppers from confocal laser scanning microscopy. *eLife* **6**, e23824 (2017).
54. A. Koehnsen, J. Kambach, S. Büsse, Step by step and frame by frame—Workflow for efficient motion tracking of high-speed movements in animals. *Zoology* **141**, 125800 (2020).

Acknowledgments: We are grateful to S. Bodenstein, H. Jeske, A. Georg, and K. Lehmann for help with the collection of the larvae and to H.-L. Tröger and M. Garitz for undergraduate research assistance. We are especially thankful for the help of L. Hindenberg, T. H. Büscher, and L. Heepe for proofreading and many elucidating discussions. Furthermore, we thank A. H. N. Dorostkar and S. N. Chegini for valuable help in power output calculations. **Funding:** This project and the work of S.B. were financed by the DFG grant BU3169/1-1. **Author contributions:** S.B. and S.N.G. designed the project and developed the concept of the study. A.K. and S.B. did the μCT analysis and postprocessing. S.B. and A.K. did the HS-Video recordings. S.B. carried out the CLSM analysis. S.B. and A.K. conducted the manipulation experiments. A.K. and S.B. did the motion tracking, developed, and tested the robotic model. H.R. calculated the power output of the system. All authors wrote the manuscript and read and approved the final version. **Competing interests:** The authors declare that they have no competing interests. **Data and materials availability:** All data supporting our findings are presented in the paper and the Supplementary Materials.

Submitted 15 May 2020
Accepted 17 December 2020
Published 20 January 2021
10.1126/scirobotics.abc8170

Citation: S. Büsse, A. Koehnsen, H. Rajabi, S. N. Gorb, A controllable dual-catapult system inspired by the biomechanics of the dragonfly larvae's predatory strike. *Sci. Robot.* **6**, eabc8170 (2021).

Science Robotics

A controllable dual-catapult system inspired by the biomechanics of the dragonfly larvae's predatory strike

Sebastian Büsse, Alexander Koehnsen, Hamed Rajabi, and Stanislav N. Gorb

Sci. Robot. **6** (50), eabc8170. DOI: 10.1126/scirobotics.abc8170

Science Robotics (ISSN 2470-9476) is published by the American Association for the Advancement of Science. 1200 New York Avenue NW, Washington, DC 20005. The title *Science Robotics* is a registered trademark of AAAS.